Tantalum oxide passivated heteroelectrodes for efficient photovoltaics and photoelectrochemical water reduction

Abstract

Crystalline silicon (c-Si) based solar cells have been dominating the photovoltaic (PV) market for decades, and c-Si based photoelectrochemical (PEC) water splitting cells have also been proven as one of the most viable alternatives for renewable production of hydrogen. Current world-record single-junction c-Si based PV and PEC devices are achieved by utilizing impurity doping within surface regions or surface deposited thin films. However, this approach leads to optoelectronic losses and high-cost processing. In this work, we employ a dopant-free tantalum oxide (TaO_x) passivated heteroelectrode architecture which provides effective protection and passivation of the c-Si surface and allows for the transport of electrons for efficient PV action and PEC water reduction. A substantial improvement in the performance of both PV and PEC devices is demonstrated, with a solar-to-electricity efficiency of 19.1% and solar-to-hydrogen efficiency of 7.7%, which corresponds to a more than 10% and a two-fold enhancement respectively. The findings presented in this paper are not limited to c-Si based devices only, and can be viewed as a general method in the interface engineering of optoelectronic and photoelectrochemical applications, with important implications for further development of dopant-free heterocathodes for high performance solar energy conversion.

Introduction

With increasing concerns over rising global energy demand and environmental sustainability, the development of renewable energy technologies is of great importance to the continuation of socio-economic development. There is growing consensus that significant contributions can come from the conversion of solar energy into electricity using photovoltaic (PV) cells and/or into chemical energy using photoelectrochemical (PEC) devices[1]. With a 90% share of global PV

market, crystalline silicon (c-Si) is unequivocally one of the most important photovoltaic technologies. Due to its high abundance in the earth crust and industrial maturity, c-Si based systems have also received significant attention for PEC applications[2-6]. Both PV and PEC devices rely on the same central working principle; photo-generated electrons and holes are separated and collected by the cell at the two opposite terminals. A common method to achieve this function is via impurity doping (i.e., boron-doped p^+ or phosphorus-doped n^+) within the near-surface regions or in surface deposited films on a silicon wafer. In spite of its remarkable success in yielding record single-junction Si solar cells (~ 26%)[7-9] and Si-based PEC water reduction (~ 13%)[10], doping involves complex fabrication processes and requires either a high thermal budget (> 800 °C) temperature, or high-vacuum plasma deposition using noxious gasses.

An attractive alternative to doping-based electrodes is the utilization of dopant-free metal-oxide-semiconductor (MOS) passivated heteroelectrodes. A typical MOS heteroelectrode is composed of a metal layer positioned on the outer surface of an oxide passivated semiconductor. To be able to function as passivated heteroelectrodes, the oxide interlayers have to fulfil several critical requirements: (i) effective passivation of defects typically present at the silicon surface, (ii) efficient transport of only one carrier type (for example electrons) and effective blocking of the other carrier (for example holes) in their path from the silicon photon absorber to the outer metal terminals, (iii) simple synthesis method at low thermal budget, (iv) transparency to broad-spectrum sunlight including free carrier absorption for application on the sunward side. Specific to PEC applications, the oxide interlayers also need to be chemically robust to survive in a very harsh aqueous environment for extended operation.

Ultrathin tunnelling silicon dioxide (SiO_2, typically ~ 1.5 nm) is one of the most well-explored oxides in heteroelectrodes for both PV[11,12] and PEC[3,5,13,14] applications, thanks to its reasonable carrier selectivity (i.e., permits the transport of collected carriers together with a low

recombination of non-collected carriers)[11,12] and its stability over a wide range of pH and chemical potentials[15]. However, the highly insulating bulk properties of SiO_2 lead to inhibition of charge transport through the MOS heteroelectrodes, restricting conduction to tunnelling or through pinholes. Furthermore, the high quality ultrathin SiO_2 places stringent requirements in film thickness control and process environment purity, leading to a small process window and a high cost of fabrication. Profound efforts have been recently devoted to explore alternative to SiO_2 interlayer to form dopant-free passivated heteroelectrodes on c-Si wafers, such as metal salts and oxides[16-22] and organic polymers[23,24].

Another system of candidate materials for dopant-free passivated heteroelectrodes are the transition metal oxides, some of which possess almost all critical characteristics for carrier selective contacts, including a wide range of work functions, semiconducting properties, and high transparency to sunlight[25]. Research on the incorporation of transition metal oxides into Si-based PV and PEC devices is very recent. High work function oxides such as molybdenum oxide, tungsten oxide, vanadium oxide and cuprous oxide have been explored as hole-selective contacts in silicon solar cells[26-31], whereas nickel oxide and cobalt oxide have been studied as effective photoanodes for water oxidation[32-34]. Interestingly, defective titanium oxide has also been reported to promote hole transport for efficient water oxidation[35,36]. In contrast, research on transition metal oxides as electron-selective contacts on crystalline silicon is scarce, with titanium oxide and strontium titanium oxide ($SrTiO_3$) so far the only transition metal oxides reported on Si solar cells[37,38] and Si photocathodes for water reduction[13], respectively.

Although it has not received as much attention yet, tantalum oxide (TaO_x) is a promising material for electron selective contacts to silicon due to: (i) small conduction band offset (~0.36 eV)[25,39], which allows electrons from the silicon conduction band to flow through the TMO, (ii) large valence band offset (~2.9eV)[25,39], which provides a barrier to prevent holes in the silicon valence band from flowing to the oxide and further to the metal cathode, and (iii) recently demonstrated effective passivation of

silicon surface defects[40,41]. In addition, TaO_x possesses high thermal and chemical stability under various pH conditions[42-45], making it a sensible photoelectrode for PEC applications. In this work, we report a nanoscale TaO_x film as a robust protection and passivated heteroelectrode for c-Si based photovoltaics and photoeletrochemical water reduction, significantly improving the solar-to-electricity and solar-to-hydrogen conversion efficiencies, respectively. We investigate the optoelectronic properties of TaO_x films synthesised by atomic layer deposition (ALD) and hydrogenated by plasma enhanced chemical vapour deposited (PECVD) silicon nitride (SiN_x), including core-level, valence band, work function, contact resistivity and surface passivation properties. We then demonstrate, for the first time, the application of hydrogenated TaO_x to Si-based PV and PEC devices for the generation of electricity and hydrogen, achieving a solar-to-electricity efficiency of 19.1% and solar-to-hydrogen efficiency of 7.7%, which corresponds to 2% and 3.8% absolute enhancement respectively over control devices without a TaO_x interlayer.

Results and Discussion

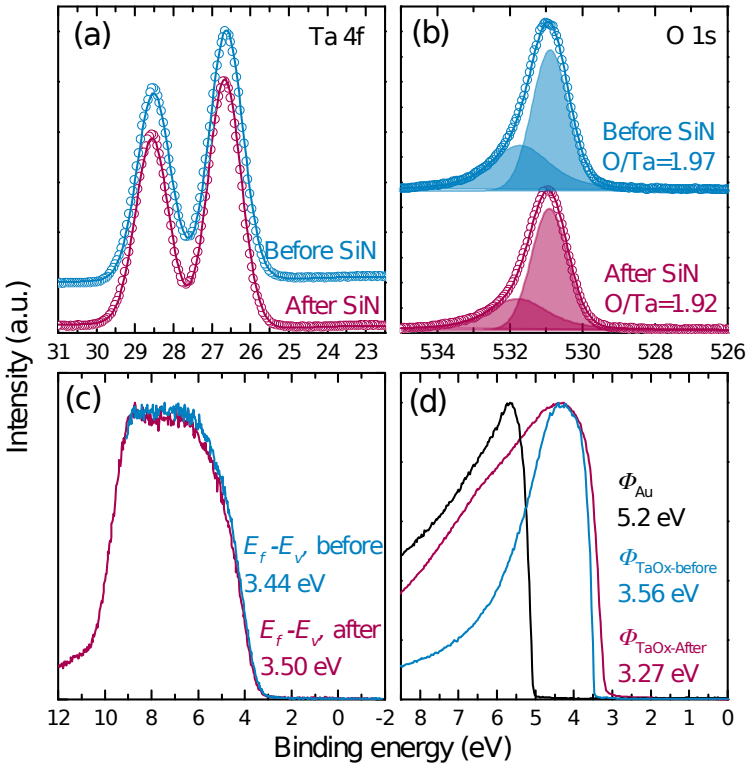

Figure 1: Electronic characterizations of atomic layer deposited TaO_x films before and after hydrogenation by silicon nitride (SiN_x). (a) and (b) present the core level spectrum of Ta 4f and O 1s, respectively. (c) shows the valence band spectrum, and (d) shows the secondary electron cut-off spectrum with a gold (Au) reference.

The TaO_x films were deposited by a thermal ALD system and hydrogenated by PECVD SiN_x (see Method section for more details). The electronic properties were characterized using X-ray photoelectron spectroscopy (XPS), where the results are shown in Figure 1. While the Ta 4f spectra shows typical doublet peaks located at 26.5 eV and 28.5 eV for Ta 4f 7/2 and Ta 4f 5/2 respectively[46], the O 1s spectra can be fitted with two Gaussian components with peaks positioned at 530.8 eV and 532 eV, respectively. The small peak located at 532 eV is usually attributed to peroxide O_2^{2-}, although sometimes it can also be due to surface contamination[46]. The component with lower binding energy peaked at 530.8 eV is from Ta-O binding[46]. Notably, the peak positions for both Ta 4f and O 1s are observed to be the same for the TaO_x film before and after SiN_x hydrogenation. However, we can notice a slight reduction in the core level peak areas of O 1s spectra after SiN_x hydrogenation. The extracted TaO_x film stoichiometry based on core level peak areas is also included in Figure 1(b). The result shows the as deposited TaO_x has an O to Ta atomic fraction of 1.97, and the TaO_x after SiN_x hydrogenation has an O to Ta atomic fraction of 1.92, implying the SiN_x hydrogenation and SiN_x etching process makes the TaO_x film slightly more sub-stoichiometric.

Figure 1(c) presents the valence band spectrum of the two TaO_x films, showing no significant difference (< 2% change). Although the TaO_x film after SiN_x hydrogenation is more metallic, no defect band in the band gap can be seen, suggesting negligible amount of filled states at the Fermi level. Further, the XPS secondary electron cut-off result shows that the TaO_x film after SiN_x hydrogenation has a work function of 3.27 eV, approximately 0.3 eV lower than that of as deposited TaO_x. The reduction of work function is expected to promote downward band-bending inside

the silicon wafer drawing electrons to the surface and consequently improving electron transport.

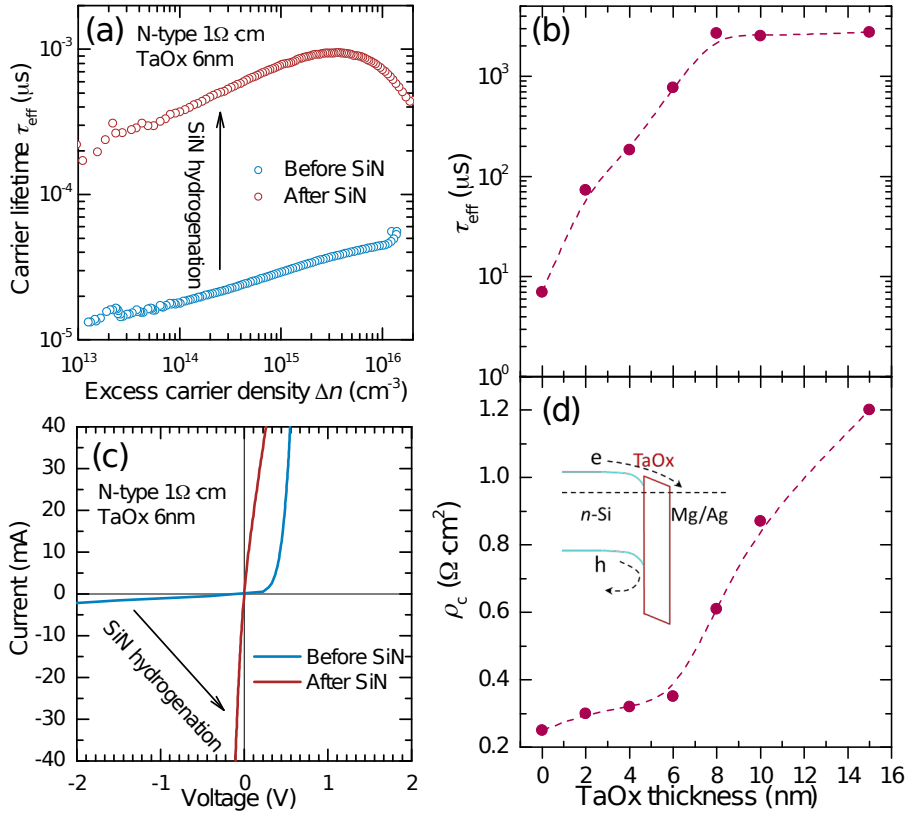

Figure 2: Carrier selectivity characterizations of TaO_x passivated heteroelectrodes to *n*-type c-Si. (a) presents the effective carrier lifetime τ_{eff} versus excess carrier density Δn for c-Si passivated with TaO_x films before and after SiN_x hydrogenation. (b) presents the effect of hydrogenated TaO_x film thickness on τ_{eff}. (c) presents a representative *I*–*V* measurements of TaO_x samples before and after SiN hydrogenation. (d) shows the effect of hydrogenated TaO_x film thickness on the contact resistivity ρ_c. The inset in (d) shows a schematic illustration of band diagram with hydrogenated TaO_x.

As mentioned above, TaO_x combines a high valence band offset, creating a potential barrier to hole transport; nevertheless, holes can still flow to the interface between TaO_x and Si, unless it is perfectly passivated. Therefore, the carrier selectivity of an *n*-Si/TaO_x hetero-structure needs to be evaluated by characterising not only the contact resistivity ρ_c but also the surface recombination velocity. A highly selective contact is achieved through a simultaneous reduction in recombination and contact resistance. One of the most straightforward techniques to probe the recombination properties of c-Si surfaces is by

measuring the effective minority carrier lifetime (τ_{eff}) of symmetrically film-passivated wafers in a contactless fashion[47] (see details in Supplementary information S1).

Figure 2(a) depicts the quality of surface passivation provided by 6 nm TaO_x films before and after SiN_x hydrogenation by plotting the injection-dependent effective carrier lifetime $\tau_{eff}(\Delta n)$ of *n*-type undiffused c-Si samples. As can be seen, the as-deposited TaO_x film (i.e., before hydrogenation) provides a poor passivation to silicon surfaces, with τ_{eff} of ~30 µs at $\Delta n = 10^{15}$ cm^{-3}. The level of surface passivation is strikingly improved more than one order of magnitude upon a SiN_x hydrogenation treatment, resulting in τ_{eff} as high as ~650 µs at $\Delta n = 10^{15}$ cm^{-3}. The enhancement in minority carrier lifetime corresponds to an increase of the internal, implied open-circuit voltage of ~150 mV (i.e., from 540 mV before to 690 mV after hydrogenation). Figure 2(b) shows that the passivation quality by hydrogenated TaO_x films depends strongly on the film thickness, where detailed injection-dependent lifetime curves are shown in Supplementary information Figure S1(b). As the TaO_x thickness increases, τ_{eff} first increases, and then tends to plateau at 8nm TaO_x. The highest lifetime achieved at $\Delta n = 10^{15}$ cm^{-3} is ~2.7 ms. The substantial enhancement in passivation upon SiN_x hydrogenation is mainly attributable to the hydrogenation of defects at the TaO_x/c-Si interface during the deposition of SiN_x[41].

Contact resistivity ρ_c was measured to evaluate the electrical current transport behaviour of the TaO_x hetero-structure[48] (see details in Supplementary information S2). Figure 2(c) shows a representative *I*–*V* measurement of TaO_x samples before and after the SiN_x hydrogenation treatment. As can be seen, the sample before SiN_x hydrogenation exhibits severe rectifying behaviour, resulting in a high contact resistivity between TaO_x and the *n*-type Si substrate. By contrast, the contact behavior of the TaO_x (~6 nm) film was enhanced dramatically upon SiN_x hydrogenation treatment, resulting in an Ohmic contact to the *n*-type Si substrate. The full series of *I*–*V* measurements are shown in Supplementary information

Figure S2(b); from that series, the ρ_c for the heteroelectrode with ~6 nm hydrogenated TaO_x is extracted to be ~0.35 Ωcm^2, which is sufficiently low to function as a full area heteroelectrode to *n*-type silicon PV and PEC devices. The high electron transport provided by the hydrogenated TaO_x on *n*-type Si can be attributed to (*i*) a reduced work function, and/or (*ii*) the Fermi-level depinning as a consequence of the passivation of interface states between TaO_x and the silicon substrate. The dependence of contact resistivity on TaO_x thickness is depicted in Figure 2(d), exhibiting a slow increase in ρ_c and then a sharp increase when TaO_x is beyond 6 nm. Indeed, when TaO_x thickness exceeds 10 nm, the contact behaves in a rectifying fashion even after the SiN_x hydrogenation. The increasing trend in both τ_{eff} and ρ_c creates a trade-off between surface passivation and contact resistivity provided by the TaO_x film. To resolve this trade-off, we fabricate completed silicon solar cells in order to find the optimum TaO_x film thickness for maximising the carrier selectivity.

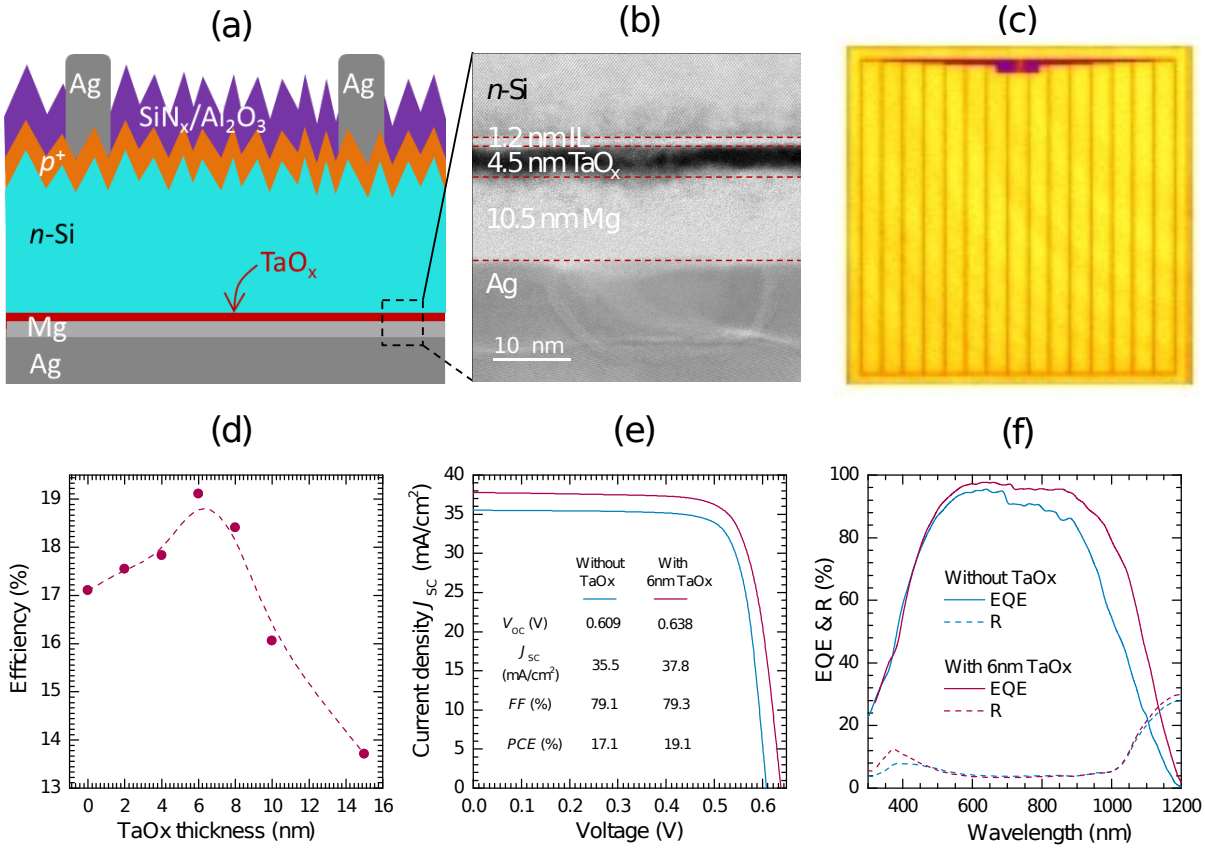

Figure 3: PV device performance with full-area rear TaO_x passivated heteroelectrodes. (a) illustrates the schematic of an *n*-type silicon solar cell featuring

full-area TaO_x at rear. (b) presents the cross-sectional transmission electron micrograph (TEM) of the rear heteroelectrodes. (c) shows photoluminescence image of the complete solar cell. (d) presents the dependence of cell efficiency on TaO_x film thickness. (e) presents the light *J–V* curves and electrical parameters of the cells with and without ~6 nm TaO_x interlayer. (f) shows the associated spectral response (external quantum efficiency and reflectance).

The complete silicon solar cells feature full area one dimension TaOx passivated heteroelectrodes and are schematically depicted in Figure 3(a). Figure 3(b) presents a cross-sectional transmission electron micrograph of the rear heteroelectrodes, showing the ~6 nm TaO_x consists of ~1.2 nm interfacial layer and ~4.5 nm TaO_x. A photoluminescence image of the complete solar cells (Figure 3c) employing a 1025 nm short-pass filter shows the cell surfaces had even optical, passivating and contact behavior. Figure 3(d) shows the solar cell power conversion efficiency as a function of TaO_x film thickness (detailed electrical parameters for these cells (V_{OC}, J_{SC}, and *FF*) are presented in Supplementary information Figure S3 and Table S3). As can be seen, the efficiency exhibits a strong dependence on TaO_x film thickness, with a maximum at a thickness of 6 nm. As TaO_x film thickness increases, the efficiency first increases primarily due to an increase in surface passivation quality and therefore an enhancement in V_{OC}, and then decreases after 6 nm mainly due to a high contact resistivity imposed by the thicker TaO_x film and therefore a reduction in *FF*. These solar cells trends are consistent with the carrier selectivity presented in Figure 2.

The light *J–V* curve for the champion cell with 6 nm TaO_x is plotted in Figure 3(e), which also includes the reference cell result without any TaO_x film. It can be seen that all cell parameters were improved drastically by inserting the 6 nm thick TaO_x layer, yielding a 19.1% solar-to-electricity conversion efficiency, which is 2% absolutely higher than the reference cell. Compared to the reference cell with metal directly on silicon, an absolute gain of 29 mV in open-circuit voltage was obtained, primarily due to the improved surface passivation provided by the hydrogenated TaO_x film. The suppression of the recombination at rear silicon surfaces also

chiefly leads to an absolute gain of 2.3 mA/cm^2 in short-circuit current. It is interesting to note that the fill factor is negligibly affected by the insertion of 6 nm TaO_x, despite of a slight increase in contact resistivity. The spectral response plotted in Figure 3(f) shows a comparable reflectance but a significant enhancement in the quantum efficiency (QE) at long wavelengths (i.e., ranges from ~900–1200 nm) for the cell with the TaO_x passivated heteroelectrode, mainly attributable to the passivation of the silicon surface by the TaO_x interlayer, and also consistent with the abovementioned improvement in lifetime, voltage and current.

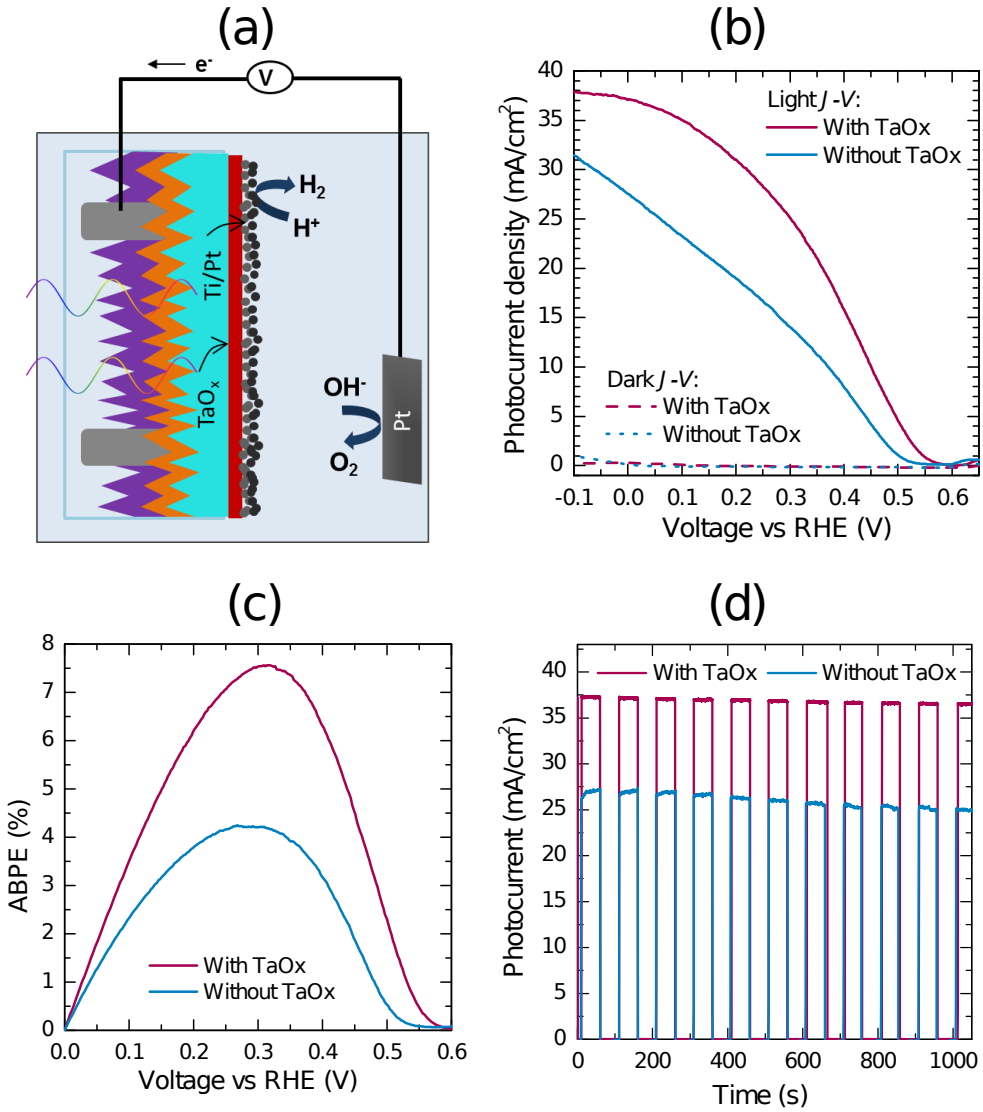

Figure 4: PEC device results with TaO_x passivated heteroelectrodes. (a) illustrates the schematic of an *n*-type silicon photocathode using TaO_x passivated

heteroelectrodes. (b) presents the photoelectrochemical current-voltage curves of Si photocathodes with and without ~6 nm TaO_x interlayer. (c) shows applied bias photon-to-current efficiency (ABPE). (d) shows amperometric current-time curves of Si photocathodes at 0V vs the reversible hydrogen electrode (RHE).

To investigate the suitability and role of TaO_x in PEC water reduction, Si photocathodes were prepared by replacing the Mg/Ag metal stack with 5 nm Ti metal and 5 nm Pt catalyst on a ~ 6 nm TaO_x film, to enable efficient hydrogen evolution reactions, as shown in Figure 4(a). Ti metal with its low work function assists in reducing the barrier between TaO_x and Pt, improving photovoltages[3]. When the TaO_x passivated silicon device is illuminated, photogenerated minority carriers (holes in this case) flow towards the illuminated p^+ region at the illuminated surface, whereas the majority carriers (electrons in this case) are transported through the TaO_x interlayer to the outer Ti/Pt catalyst, where hydrogen evolution reaction takes place. An advantage of this MOS passivated heteroelectrode design is the decoupling of photon absorption and hydrogen reduction reaction, enabling the independent optimisation of light harvesting and catalytic performance of the electrodes.

For comparison, a reference Si-based photocathode was prepared without TaO_x film. Figure 4(b) compares the photoelectrochemical performance of Si photocathodes with and without TaO_x. The reference Si photoelectrode shows an onset potential of 525 mV whereas the photoelectrode with ~ 6 nm of TaO_x showed a more positive onset potential of 565 mV for water reduction. Photocurrent density of the TaO_x protected and passivated electrode reaches 37.1 mA/cm^2 at 0V vs RHE, compared to the 27.5 mA/cm^2 obtained on the reference photoelectrode without TaO_x interlayer. The significant enhancement in photocurrents and photovoltages are attributed to the high carrier selectivity of TaO_x suppressing the carrier recombination whilst maintaining efficient electron transport. This result is also consistent with the photovoltaic characteristics as shown in Figure 3. Applied bias photon-to-current efficiency (ABPCE) has reached 7.7% which is one of the best reported for dopant-free Si photoelectrodes without highly doped Si contact layers. The

solar-to-hydrogen conversion efficiency of TaO_x/Si based MOS photocathodes remains below the solar-to-electricity conversion efficiencies of the Si PV counterparts as shown in Figure 3, mainly due to lower photovoltage and *FF* of the PEC devices. Beyond the thermodynamic energy loss associated with the water reduction electrolyte, this disparity can be largely attributed to unfavourable energy band alignment in Ti/TaO_x/Si MOS photocathode compared to Mg/TaO_x/Si MOS architecture in PV cells, leading to high barrier height for electron transport and therefore causing significant loss in the electron selectivity (that is higher recombination and contact resistivity).

As the electrodes used for water splitting must endure highly corrosive and reducing environment, a stability test has been carried out to evaluate the photoresponse and photostability. As shown in Figure 4(d), the electrodes showed fast photoresponse during light on-off cycles. However, the reference electrode exhibited slight drop in photocurrents with time while the photoelectrode with TaO_x film showed highly stable photoresponse. It is known that c-Si is stable in acid environments while it is highly unstable in oxidising conditions. The instability of the reference electrode is attributed to the lack of hole blocking effect at the interface, inducing possible self-oxidising conditions. The long-term stability of TaO_x is further evaluated in 1M hydrochloric acid solution for 2 hours of continuous operation (see Supplementary information Figure S4). TaO_x possesses exceptional thermal and chemical stability under various pH conditions[42,43]. Due to its wide bandgap, TaO_x does not compete with the underlying absorber for light absorption. Combined with its passivation effect, TaO_x as a protection and passivation interlayer can be instrumental in protecting various semiconductor photocathodes in harsh environments while improving photoelectrochemical performance by selectively collecting electrons.

Conclusion

In summary, we have demonstrated a nanoscale TaO_x passivated heteroelectrode for c-Si based photovoltaics and photoeletrochemical

water reduction. We have achieved a solar-to-electricity efficiency of 19.1% and a solar-to-hydrogen efficiency of 7.7%, which corresponds to 2% and 3.8% absolute enhancement, respectively over the control devices without the TaO_x interlayer. The solar-to-hydrogen efficiency is so far the highest reported ABPE for the dopant-free single-junction silicon photocathodes, and additional improvement can be anticipated with further optimisation of the carrier selectivity of TaO_x passivated heteroelectrode and adaption of advanced silicon solar cells structure, for example, the heterojunction back contacted solar cells which hold the current world-record conversion efficiency. The finding is not limited to the TaO_x/Si platform and should provide a general method in the interface engineering of optoelectronic and photoelectrochemical applications.

Method

The TaO_x films were deposited by a thermal ALD reactor (Picosun, R200 Advanced) using Tantalum Ethoxide precursor at 250 °C and had a corresponding growth rate of 0.35 Å/cycle as measured by ex-situ spectroscopic ellipsometry (J.A. Woolam M2000 ellipsometer). The hydrogenation of TaO_x film was realised by capping PECVD SiN_x atop TaO_x and then stripping off the SiN_x layer by 1% hydrofluoric acid, taking advantage of the exceptional chemical stability of TaO_x film under various pH conditions. PECVD SiN_x has been well-known in providing hydrogen to manipulate bulk and interfacial properties of a range of materials such as silicon[49]. The capping SiN_x layer was deposited in a microwave/radio-frequency PECVD reactor (AK400, Roth & Rau)[50], having a thickness of 85 nm and a refractive index of ~1.9 at 632 nm.

Further details are given in the Supplementary Information.

References

1. Walter, M. G. *et al.* Solar Water Splitting Cells. *Chemical Reviews* **110**, 6446-6473, (2010).
2. Sun, K. *et al.* Enabling Silicon for Solar-Fuel Production. *Chemical Reviews* **114**, 8662-8719, (2014).
3. Esposito, D. V., Levin, I., Moffat, T. P. & Talin, A. A. H2 evolution at Si-based metal–insulator–semiconductor photoelectrodes enhanced by inversion channel charge collection and H spillover. *Nat Mater* **12**, 562-568, (2013).
4. Reece, S. Y. *et al.* Wireless Solar Water Splitting Using Silicon-Based Semiconductors and Earth-Abundant Catalysts. *Science* **334**, 645-648, (2011).
5. Ji, L. *et al.* Localized dielectric breakdown and antireflection coating in metal-oxide-semiconductor photoelectrodes. *Nat Mater* **16**, 127-131, (2017).

6. Zhou, X. *et al.* 570 mV photovoltage, stabilized n-Si/CoOx heterojunction photoanodes fabricated using atomic layer deposition. *Energy & Environmental Science* **9**, 892-897, (2016).
7. Zhao, J. Recent advances of high-efficiency single crystalline silicon solar cells in processing technologies and substrate materials. *Solar Energy Materials and Solar Cells* **82**, 53-64, (2004).
8. Glunz, S. *et al.* in *31st European Photovoltaic Solar Energy Conference and Exhibition.*
9. Masuko, K. *et al.* Achievement of More Than 25% Conversion Efficiency With Crystalline Silicon Heterojunction Solar Cell. *Photovoltaics, IEEE Journal of* **4**, 1433-1435, (2014).
10. Wang, H.-P. *et al.* High-Performance a-Si/c-Si Heterojunction Photoelectrodes for Photoelectrochemical Oxygen and Hydrogen Evolution. *Nano Letters* **15**, 2817-2824, (2015).
11. Godfrey, R. B. & Green, M. A. 655 mV open-circuit voltage, 17.6% efficient silicon MIS solar cells. *Applied Physics Letters* **34**, 790-793, (1979).
12. Green, M. A. & Blakers, A. W. Advantages of metal-insulator-semiconductor structures for silicon solar cells. *Solar Cells* **8**, 3-16, (1983).
13. Ji, L. *et al.* A silicon-based photocathode for water reduction with an epitaxial SrTiO3 protection layer and a nanostructured catalyst. *Nat Nano* **10**, 84-90, (2015).
14. Hill, J. C., Landers, A. T. & Switzer, J. A. An electrodeposited inhomogeneous metal-insulator-semiconductor junction for efficient photoelectrochemical water oxidation. *Nat Mater* **14**, 1150-1155, (2015).
15. Pourbaix, M. *Atlas of Electrochemical Equilibria in Aqueous Solutions*. 2nd edn edn, 458_463 (National Association of Corrosion Engineers, 1974).
16. Zhang, Y., Liu, R., Lee, S.-T. & Sun, B. The role of a LiF layer on the performance of poly(3,4-ethylenedioxythiophene):poly(styrenesulfonate)/Si organic-inorganic hybrid solar cells. *Applied Physics Letters* **104**, 083514, (2014).
17. Bullock, J. *et al.* Efficient silicon solar cells with dopant-free asymmetric heterocontacts. *Nature Energy* **1**, (2016).
18. Bullock, J. *et al.* Lithium Fluoride Based Electron Contacts for High Efficiency n-Type Crystalline Silicon Solar Cells. *Advanced Energy Materials*, (2016).
19. Wan, Y. *et al.* Magnesium fluoride electron–selective contacts for crystalline silicon solar cells. *ACS applied materials & interfaces*, (2016).
20. Zhang, Y. *et al.* High efficiency hybrid PEDOT:PSS/nanostructured silicon Schottky junction solar cells by doping-free rear contact. *Energy & Environmental Science* **8**, 297-302, (2015).
21. Bullock, J. *et al.* in *IEEE 43rd Photovoltaic Specialist Conference (PVSC).*
22. Wan, Y. *et al.* Conductive and Stable Magnesium Oxide Electron-Selective Contacts for Efficient Silicon Solar Cells. *Advanced Energy Materials* **7**, 1601863-n/a, (2017).
23. Schmidt, J., Titova, V. & Zielke, D. Organic-silicon heterojunction solar cells: Open-circuit voltage potential and stability. *Applied Physics Letters* **103**, 183901, (2013).
24. Zhang, Y. *et al.* Heterojunction with organic thin layers on silicon for record efficiency hybrid solar cells. *Advanced Energy Materials* **4**, (2014).
25. Greiner, M. T. *et al.* Universal energy-level alignment of molecules on metal oxides. *Nat Mater* **11**, 76-81, (2012).
26. Battaglia, C. *et al.* Silicon heterojunction solar cell with passivated hole selective MoOx contact. *Applied Physics Letters* **104**, 113902, (2014).
27. Battaglia, C. *et al.* Hole selective MoO x contact for silicon solar cells. *Nano letters* **14**, 967-971, (2014).
28. Bivour, M., Temmler, J., Steinkemper, H. & Hermle, M. Molybdenum and tungsten oxide: High work function wide band gap contact materials for hole selective contacts of silicon solar cells. *Solar Energy Materials and Solar Cells* **142**, 34-41, (2015).
29. Bullock, J., Cuevas, A., Allen, T. & Battaglia, C. Molybdenum oxide MoOx: A versatile hole contact for silicon solar cells. *Applied Physics Letters* **105**, 232109, (2014).
30. Geissbühler, J. *et al.* 22.5% efficient silicon heterojunction solar cell with molybdenum oxide hole collector. *Applied Physics Letters* **107**, 081601, (2015).
31. Zhang, X., Wan, Y., Bullock, J., Allen, T. & Cuevas, A. Low resistance Ohmic contact to p-type crystalline silicon via nitrogen-doped copper oxide films. *Applied Physics Letters* **109**, 052102, (2016).
32. Chen, L. *et al.* p-Type Transparent Conducting Oxide/n-Type Semiconductor Heterojunctions for Efficient and Stable Solar Water Oxidation. *Journal of the American Chemical Society* **137**, 9595-9603, (2015).
33. Kenney, M. J. *et al.* High-Performance Silicon Photoanodes Passivated with Ultrathin Nickel Films for Water Oxidation. *Science* **342**, 836-840, (2013).
34. Sun, K. *et al.* Nickel oxide functionalized silicon for efficient photo-oxidation of water. *Energy & Environmental Science* **5**, 7872-7877, (2012).
35. Chen, Y. W. *et al.* Atomic layer-deposited tunnel oxide stabilizes silicon photoanodes for water oxidation. *Nat Mater* **10**, 539-544, (2011).
36. Hu, S. *et al.* Amorphous TiO₂ coatings stabilize Si, GaAs, and GaP photoanodes for efficient water oxidation. *Science* **344**, 1005-1009, (2014).
37. Allen, T. G. *et al.* A Low Resistance Calcium/Reduced Titania Passivated Contact for High Efficiency Crystalline Silicon Solar Cells. *Advanced Energy Materials*, 1602606-n/a, (2017).
38. Avasthi, S. *et al.* Hole-blocking titanium-oxide/silicon heterojunction and its application to photovoltaics. *Applied Physics Letters* **102**, 203901, (2013).
39. Robertson, J. & Chen, C. W. Schottky barrier heights of tantalum oxide, barium strontium titanate, lead titanate, and strontium bismuth tantalate. *Applied Physics Letters* **74**, 1168-1170, (1999).
40. Wan, Y., Bullock, J. & Cuevas, A. Passivation of c-Si surfaces by ALD tantalum oxide capped with PECVD silicon nitride. *Solar Energy Materials and Solar Cells* **142**, 42-46, (2015).
41. Wan, Y., Bullock, J. & Cuevas, A. Tantalum oxide/silicon nitride: A negatively charged surface passivation stack for silicon solar cells. *Applied Physics Letters* **106**, 201601, (2015).
42. Anderson, M. D., Aitchison, B. & Johnson, D. C. Corrosion Resistance of Atomic Layer Deposition-Generated Amorphous Thin Films. *ACS applied materials & interfaces* **8**, 30644-30648, (2016).
43. Li, C., Wang, T., Luo, Z., Zhang, D. & Gong, J. Transparent ALD-grown Ta2O5 protective layer for highly stable ZnO photoelectrode in solar water splitting. *Chemical communications* **51**, 7290-7293, (2015).

44. Chen, S. & Wang, L.-W. Thermodynamic Oxidation and Reduction Potentials of Photocatalytic Semiconductors in Aqueous Solution. *Chemistry of Materials* **24**, 3659-3666, (2012).
45. Hu, S. *et al.* Thin-Film Materials for the Protection of Semiconducting Photoelectrodes in Solar-Fuel Generators. *The Journal of Physical Chemistry C* **119**, 24201-24228, (2015).
46. Atanassova, E. & Spassov, D. X-ray photoelectron spectroscopy of thermal thin Ta2O5 films on Si. *Applied Surface Science* **135**, 71-82, (1998).
47. Sinton, R. A. & Cuevas, A. Contactless determination of current--voltage characteristics and minority-carrier lifetimes in semiconductors from quasi-steady-state photoconductance data. *Applied Physics Letters* **69**, 2510-2512, (1996).
48. Cox, R. H. & Strack, H. Ohmic contacts for GaAs devices. *Solid-State Electronics* **10**, 1213-1218, (1967).
49. Aberle, A. G. Overview on SiN surface passivation of crystalline silicon solar cells. *Solar Energy Materials and Solar Cells* **65**, 239-248, (2001).
50. Wan, Y., McIntosh, K. R. & Thomson, A. F. Characterisation and optimisation of PECVD SiNx as an antireflection coating and passivation layer for silicon solar cells. *AIP ADVANCES* **3**, 032113, (2013).

Acknowledgements
This work was supported by the Australian Government through the Australian Research Council (Discovery Project: DP150104331). Some facilities at the Australian National Fabrication Facility and Centre for Advanced Microscopy at ANU were used. XPS characterization was performed at the Joint Center for Artificial Photosynthesis, supported through the Office of Science of the US Department of Energy under Award Number DE-SC0004993. AJ, MH and JB acknowledge funding from the Bay Area Photovoltaics Consortium (BAPVC).

Author contributions

Additional information
The authors declare no competing financial interests. Correspondence and requests for materials should be addressed to Y.W.